Environmental Science Nano

# Reciprocal Redox Interactions of Lithium Cobalt Oxide Nanoparticles with Nicotinamide Adenine Dinucleotide (NADH) and Glutathione (GSH): Toward a Mechanistic Understanding of Nanoparticle-Biological Interactions



| | |
|---|---|
| Journal: | *Environmental Science: Nano* |
| Manuscript ID | EN-ART-12-2020-001221.R1 |
| Article Type: | Paper |
| | |

Environmental Significance Statement:

The environmental impact of nanomaterials can be strongly modulated by their chemical transformations. Despite the critical role that redox chemistry plays in biology, the influence of specific biologically relevant electron transporters such as nicotinamide adenine dinucleotide (NADH) and glutathione (GSH) on the transformation of engineered nanoparticles, and the reciprocal influence of nanoparticles on the oxidation state of these molecules, have not been widely considered previously. The present work shows that the exposure of $LiCoO_2$ nanoparticles to nicotinamide adenine dinucleotide (NADH) accelerates release of $Co^{2+}$ by reducing cobalt from its highly insoluble $Co^{3+}$ form to the soluble $Co^{2+}$ form, and the $LiCoO_2$ concurrently oxidizes NADH to $NAH^{+}$. Similar results are observed using glutathione. Transformations of nanoparticles driven by redox chemistry of molecules involved in biological electron transport pose two important mechanisms for toxicity in the environment. First, the reduction of Co(III) and other high-valence metals to lower-valence states increases their solubility and leads to faster release into the aqueous phase. Secondly, the corresponding reciprocal oxidation of NADH, GSH, and other molecules relevant to electron transport and cellular homeostasis can serve as a direct pathway to biological impact.

ARTICLE

# Reciprocal Redox Interactions of Lithium Cobalt Oxide Nanoparticles with Nicotinamide Adenine Dinucleotide (NADH) and Glutathione (GSH): Toward a Mechanistic Understanding of Nanoparticle-Biological Interactions

Received 00th January 20xx,
Accepted 00th January 20xx

DOI: 10.1039/x0xx00000x

Austin H. Henke,[a] Elizabeth D. Laudadio,[a] Jenny K. Hedlund Orbeck,[a] Ali Abbaspour Tamijani,[b] Khoi Nguyen L. Hoang,[c] Sara E. Mason,[b] Catherine J. Murphy,[c] Z. Vivian Feng,[d] Robert J. Hamers*[a]

Among high-valence metal oxides, $LiCoO_2$ and related materials are of environmental importance because of the rapidly increasing use of these materials as cathodes in lithium ion batteries. Understanding the impact of these materials on aqueous environments relies on understanding their redox chemistry because Co release is dependent on oxidation state. Despite the critical role that redox chemistry plays in cellular homeostasis, the influence of specific biologically relevant electron transporters such as nicotinamide adenine dinucleotide (NADH) and glutathione (GSH) on the transformation of engineered nanoparticles has not been widely considered previously. Here we report an investigation of the interaction of $LiCoO_2$ nanoparticles with NADH and GSH. Measurements of Co release using inductively coupled plasma-mass spectrometry (ICP-MS) show that exposing $LiCoO_2$ nanoparticles to either NADH or GSH increases solubilization of cobalt, while corresponding spectroscopic measurements show that NADH is concurrently oxidized to $NAD^+$. To demonstrate that these effects are a consequence the high-valence Co(III) in $LiCoO_2$ nanoparticles, we performed control experiments using Co(II)-containing $Co(OH)_2$ and $LiCoPO_4$, and dissolved $Co^{2+}/Li^+$ ions. Additional experiments using molecules of similar structure to NADH and GSH, but that are not reducing agents, confirm that these transformations are driven by redox reactions and not by chelation effects. Our data show that interaction of $LiCoO_2$ with NADH and GSH induces release $Co^{2+}$ ions and alters the redox state of these biologically important transporters. Observation of NADH binding to $LiCoO_2$ using x-ray photoelectron spectroscopy (XPS) suggests a surface catalyzed reaction. The reciprocal reduction of $LiCoO_2$ to enable release of $Co^{2+}$ and corresponding oxidation of NADH and GSH as model redox-active biomolecules has implications for understanding the biological impacts of high-valence metal oxide nanomaterials.

## 1. Introduction

The interactions of nanomaterials with environmental and biological systems involve a complex suite of interaction mechanisms. While physical interactions can be important, many emerging nanoparticles of technological utility have chemical compositions that are reactive, leading to new mechanisms such as release of solubilized metals[1, 2] or surface-driven formation of reactive oxygen species. For example, nano-Ag(0) can be oxidized to Ag(I), which then has significant antimicrobial activity. Metal oxides constitute the most widely used class of engineered nanomaterials and are frequently used in high oxidation states, with the corresponding metal hydroxides having much lower solubility than those formed from the lower oxidation states. For example, at pH = 6, the solubility of $Fe(OH)_3$ is ~$10^{-13}$ M while $Fe(OH)_2$ is highly soluble. Because of the low solubility of high-valence metals, redox-active small organic acids can enhance dissolution of metal oxides by reducing the metals to lower oxidation states,[3-7] and biologically-induced reduction processes impact biogeochemical cycling of metals such as Fe and Mn.[8-10] The interaction of biomolecular reducing agents with nanoparticles could induce biological impacts both by enhancing release of transition metals and by altering the cellular redox potential and associated homeostasis. Despite the critical role that redox chemistry plays in cellular homeostasis, the influence of specific biologically relevant electron transporters such as nicotinamide adenine dinucleotide (NADH) and glutathione (GSH) on the transformation of engineered nanoparticles has not been widely considered previously.

Among high-valence metal oxides, $LiCoO_2$ and a broader family of "NMC" compositions ($LiNi_xMn_yCo_{1-x-y}O_2$, x,y < 1) are of particular environmental importance because of the rapidly

[a] Department of Chemistry, University of Wisconsin, Madison, USA.
[b] Department of Chemistry University of Iowa, Iowa City, Iowa, USA.
[c] Department of Chemistry, University of Illinois, Urbana-Champaign, USA.
[d] Department of Chemistry, Augsburg University, Minneapolis, USA.

†Electronic Supplementary Information (ESI) available: (1) Nanoparticle synthesis procedures, (2) description of XPS calculations, (3) DFT computational details, (4) minimal medium composition and chemical information, (5) changes in solution pH before/after nanoparticle exposure, (6) fluorescence and ICP-MS calibration, (7) TEM images of $LiCoO_2$ nanoparticles, (8) quantified [Li] release determined by ICP-MS, (9) comparison of NADH and $NAD^+$ fluorescence spectra, (10) representative x-ray photoelectron spectra for NADH binding to nanoparticles, (11) additional control experiments regarding NADH fluorescence, and (12) additional control experiments regarding NADH/$NAD^+$ UV-visible spectra. See DOI: 10.1039/x0xx00000x

increasing use of these materials in micro- and nano-structured form as cathodes in lithium-ion batteries. Because the use of lithium ion batteries in consumer electronics is rapidly expanding and their recycling is limited,[11] understanding the chemical transformations of $LiCoO_2$ has significant potential for environmental risk assessment and provides fundamental insights of a broader class of high-valence transition metal nanoparticles. Released cobalt from $LiCoO_2$ is hazardous to cells in aqueous environments because it is carcinogenic, induces oxidative stress, competes with the intended ions (e.g. $Fe^{2+}$) for binding sites in metalloproteins, induces a hypoxia-like state, and has increased mobility once in the Co(II) form.[12, 13] Cobalt is released in a manner strongly dependent on the oxidation state. At pH = 6, the solubility of $Co^{3+}$ is ~$1x10^{-20}$ M compared with >$10^{-5}$ M for $Co^{2+}$, based on the experimental solubility products of $Co(OH)_3$ and $Co(OH)_2$.[14, 15] Among redox-active biomolecules that could impact $LiCoO_2$ dissolution, the NADH/$NAD^+$ and GSH/GSSG redox couples, depicted in Figure 1, are among the most important. NADH can be oxidized to $NAD^+$, while GSH can be oxidized to glutathione disulfide (GSSG) by forming a disulfide dimer. Both NADH/$NAD^+$ and GSH/GSSG act as coenzymes and substrates for various metabolic processes and maintain an appropriate redox state within the cell (e.g. antioxidants).[16, 17]

Here we report an investigation of the interaction between $LiCoO_2$ nanoparticles with NADH and GSH. Between these molecules, we choose to primarily study NADH with some comparison to GSH. Prior studies have shown surface-mediated oxidation of GSH on nanocarbon surfaces.[18, 19] NADH or GSH may interact is such a way with $LiCoO_2$, which to our knowledge has not been reported. Additionally, the redox-dependent fluorescence of NADH/$NAD^+$ allows for easy detection, making the molecule an appealing choice. Quantitative measurements of Co release using inductively coupled plasma-mass spectrometry (ICP-MS) show that exposure of $LiCoO_2$ nanoparticles to either NADH or GSH increases solubilization of cobalt, while corresponding spectroscopic measurements show that NADH is concurrently oxidized to $NAD^+$. To demonstrate that these effects are a consequence of the high valence of Co(III) in $LiCoO_2$, we performed control experiments using Co(II)-containing $Co(OH)_2$ and $LiCoPO_4$. Additionally, by testing interaction of $LiCoO_2$, etc. with molecules of similar structure to NADH and GSH, but that are not reducing agents, we find the NADH oxidation / Co reduction effect due to a redox reaction and not chelation of a specific functional group with Co or the dissolved ions. This coupled transformation of $LiCoO_2$ and redox-active biomolecules has implications in the biological impacts of high-valence metal oxide nanomaterials and the redox-driven weathering of metal oxides.

## 2. Experimental

### 2.1 Nanoparticle synthesis and characterization

We synthesized sheet-like nanoparticles of cobalt hydroxide, $Co(OH)_2$, and $LiCoO_2$ following procedures we described previously.[20, 21] $Co(OH)_2$ nanosheets were prepared via a precipitation method. The $Co(OH)_2$ precursor was converted to $Li_xCoO_2$ using a molten salt flux of 6:4 molar ratio of $LiNO_3$:LiOH at 200 °C. As a control sample, we synthesized rod-like Cmcm $LiCoPO_4$ nanoparticles using a microwave-assisted solvothermal method adapted from a method published previously.[22] All solutions in this study were prepared from nanopure water (Barnstead Genpure System, ρ ≥ 18.2 MΩ·cm). Detailed procedures for nanoparticle syntheses and chemical information (Table S1) can be found in the Electronic Supplementary Information (ESI†).

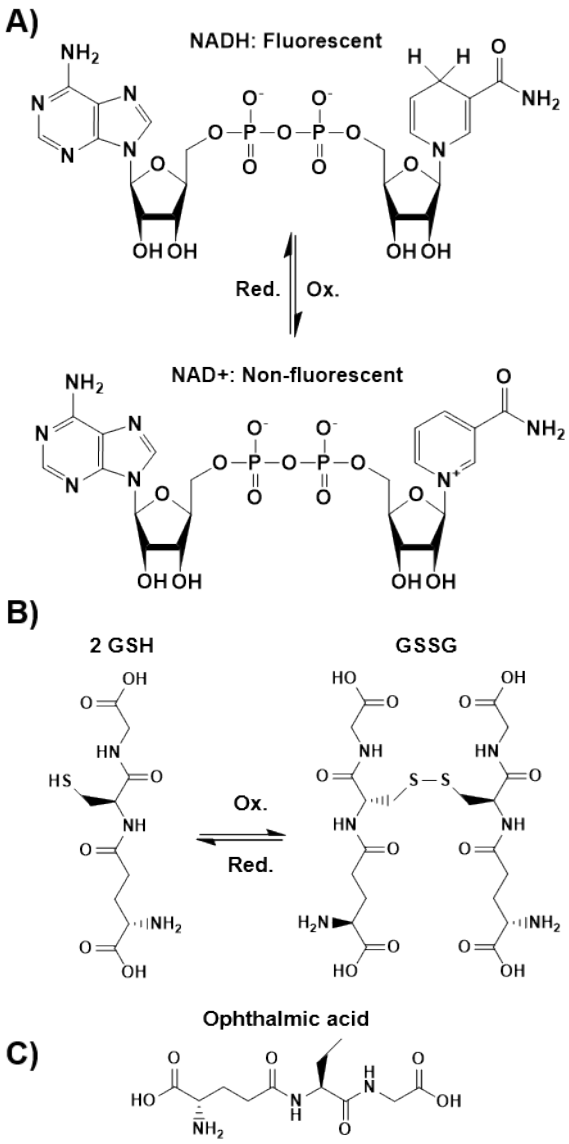


**Figure 1.** Oxidation-reduction equilibria ($H^+$ not shown) of the biomolecules A) NADH and $NAD^+$, B) glutathione (GSG) and glutathione disulfide (GSSG), and C) structure of ophthalmic acid (OA), a molecule similar to glutathione except lacking the redox-active thiol moiety.

Powder X-ray diffraction (XRD) patterns were obtained for each sample using a Bruker D8 Advance diffractometer equipped with a copper $K_\alpha$ source and 6 mm slit width. Samples for XRD analysis were prepared by affixing nanoparticle powder onto a B-doped silicon crystal zero-diffraction plate (MTI

Corporation) with vacuum grease. Scanning electron microscope (SEM) images were collected using a LEO Supra55 VP field-emission scanning electron microscope. Samples for SEM were prepared by drop-casting a dilute solution of nanoparticles suspended in ethanol onto a conductive B-doped silicon wafer. Specific surface area measurements of ~0.1 g vacuum-dried samples were determined by nitrogen physisorption (Micromeritics Gemini VII 2390 surface area analyzer) and Brunauer-Emmett-Teller (BET) analysis.[23] Lastly, we used dynamic light scattering (DLS) and laser Doppler microelectrophoresis with a Malvern Zetasizer Nano ZS to measure particle aggregate size and surface charge (respectively) in the solution of interest. Each particle type was suspended in minimal medium with dextrose (see section 2.2) at 100 mg·mL$^{-1}$ in approximately 10 mL. These stock solutions were then diluted to 5 mg·mL$^{-1}$. Particle suspensions were sonicated for 1 h in a cup ultrasonicator with cooling water (10 s on, 10 s off for 30 min total sonication time) immediately before analysis. The results reported are averages and standard errors of the mean of at least three measurements of size (number mean) and zeta potential for each sample.

**2.2 Dissolution studies with nanoparticles and biomolecules**

A model bacterial growth medium with minimal constituents ("minimal medium" with dextrose) was prepared in nanopure water with various salts, 4-(2-hydroxyethyl)-1-piperazineethanesulfonic acid (HEPES) buffer, and dextrose. See Table S1 for chemical information and Table S2 for the full composition of minimal medium with dextrose in the ESI†. We recognize that minimal medium used may not fully replicate the complex environment inside cells, perhaps warranting further investigations. However, this medium does provide a relatively simple matrix to investigate the specific interactions of NADH and other molecules with the nanomaterials of interest. Additionally, while NADH is typically unable to transverse membranes, there is evidence that lower concentrations of NADH can exist in extracellular matrices via transmembrane protein transport or other mechanisms.[24] It follows that our conclusions do not rely on nanomaterials entering cells.

NADH reduced disodium salt, NAD$^+$ free acid, L-glutathione reduced, and ophthalmic acid were obtained from Sigma Aldrich and used as received. Ophthalmic acid (OA) is nearly identical to glutathione in structure, except it lacks the redox-active thiol group (Figure 1C). Solutions were prepared for each molecule of interest by dissolving 0.5 mM in minimal medium. This concentration was chosen because it is relevant to concentrations of these molecules found in certain cells[25-27] and produces suitable fluorescence and absorbance signals for NADH/NAD$^+$ solutions. Nanoparticles were introduced to each solution at 1 mg·mL$^{-1}$ nanoparticle concentration, using vials of approximately 3 mL. The sealed vials were covered from light and shaken for 24 h. The samples were then centrifuged at 13,100 × g for 20 min (Eppendorf MiniSpin plus). Finally, the supernatant was collected and filtered through 0.1 µm porosity syringe filter cartridges (Millex VV) to ensure nanoparticle removal. Preliminary experiments in which particles were isolated only by centrifugation saw remaining particles cause light scattering in fluorescence measurements, particularly for $LiCoO_2$. Light scattering was eliminated with the introduction of the additional syringe filter isolation step. While the 0.1 µm porosity dimension is larger than certain particle dimensions, most particles are likely blocked as aggregates while navigating the filter. All experiments were performed in at least duplicate and error bars represent standard error of the mean.

We performed another form of dissolution experiment to study the reaction kinetics of NADH and $LiCoO_2$ in a single solution over time. $LiCoO_2$ was introduced at 1 mg·mL$^{-1}$ to a single 30 mL solution of NADH in minimal medium in a larger reaction vessel. The reaction was stirred for 48 h total, and 1-mL aliquots were removed at 2 h, 6 h, 12 h, 24 h, and 48 h (five total). The 1 mg·mL$^{-1}$ concentration for $LiCoO_2$ does change vary greatly from aliquot removal because the volume change (1 mL) is small relative to the total volume (30 mL) and the stirred solution is moderately homogeneous. The aliquots were centrifuged and filtered in the same way as the above samples.

**2.3 Quantification of NADH concentrations**

The concentration of NADH in samples was determined using fluorescence measurements using an ISS K2 photon-counting spectrofluorimeter, using measurement conditions similar to those reported previously.[28, 29] Samples were placed in a fused silica cuvette at room temperature, excited at $\lambda_{ex}$ = 338 nm, and the emission spectrum was measured between $\lambda_{em}$ = 400 and $\lambda_{em}$ =550 nm with a step size $\Delta\lambda$ = 1 nm and integration time of 1 s per step. NADH exhibits an emission peak at $\lambda_{ex} \approx$ 455 nm, whereas NAD$^+$ does not. The intensity was background-subtracted using a blank consisting of minimal medium with dextrose. Spectra were also normalized to the fluorescence of a solid tetraphenylbutadiene (TPB) standard to account for day-to-day variations in lamp intensity. NADH was quantified by converting the fluorescence intensity to concentration using a calibration curve (Figure S1, ESI†). As a secondary method for detecting NADH and NAD$^+$, UV-visible absorbance spectra were obtained of selected NADH and NAD$^+$ solutions using a Shimadzu UV2401 dual-beam spectrophotometer.

**2.4 Determination of dissolved ion concentrations**

We used inductively coupled plasma mass spectrometry (ICP-MS, Shimadzu 2030) to measure dissolved ion concentrations in samples after centrifugation/filtration. Samples were acidified in 2.5% $HNO_3$ before analysis. Additionally, a 500:1 dilution was required to reduce salt concentrations from the minimal medium. $^7$Li and $^{59}$Co intensities were measured and referenced to internal standards of $^9$Be and $^{69}$Ga, respectively. Each sample was measured in triplicate by ICP-MS and the average intensities were used for quantification. Concentrations of Li and Co were determined using calibration curves (Figure S2, ESI†). Standard solutions of Li and Co (combined) were

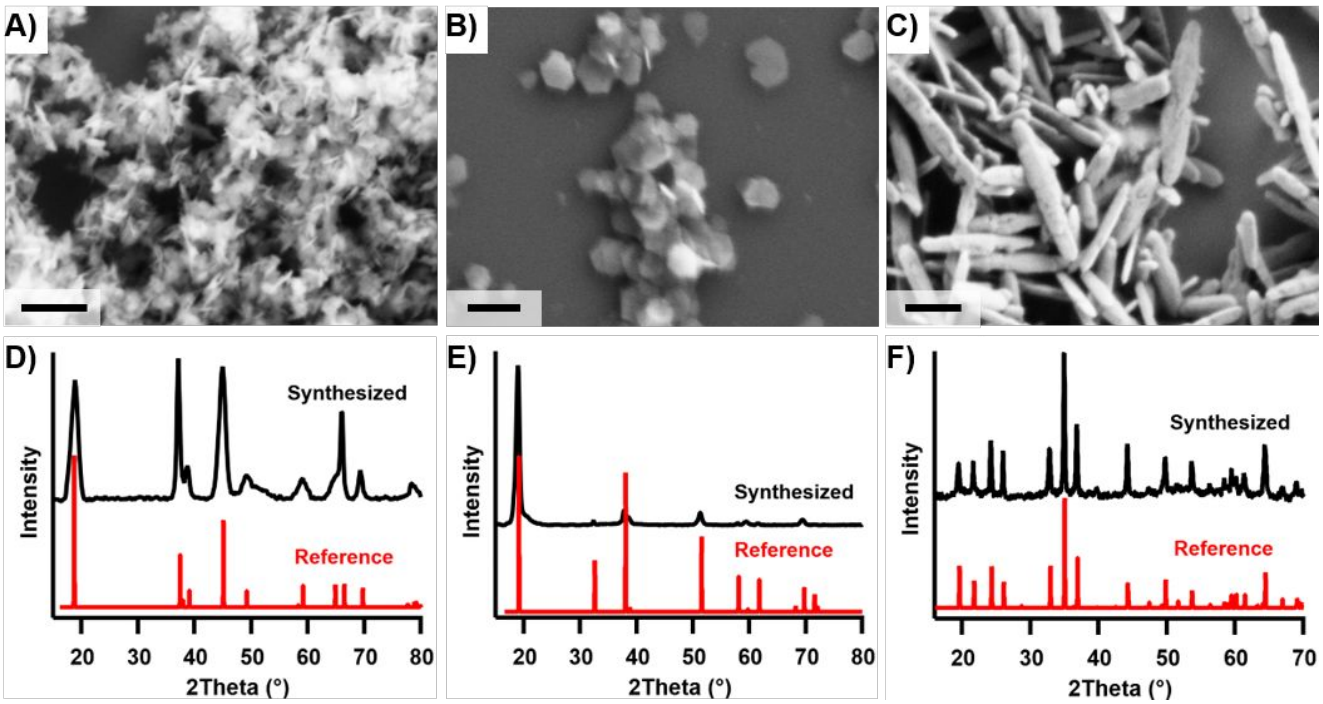


**Figure 2.** Scanning electron microscopy images and x-ray diffraction patterns for A/D) $LiCoO_2$, B/E) $Co(OH)_2$, and C/F) $LiCoPO_4$ nanoparticles, respectively. Scale Bars = 200 nm. Experimental XRD patterns (black) are compared to reference patterns (red). See text for references.

prepared by serial dilution from 1 $g \cdot L^{-1}$ certified reference materials. Standards were diluted and acidified in the same manner as the unknowns.

### 2.5 Nanoparticle-NADH binding experiments

To examine if NADH/$NAD^+$ bind to nanoparticles surfaces, we used X-ray photoelectron spectroscopy to characterize the surface composition of nanoparticles that were exposed to NADH in nanopure water. Nanopure water was used instead of minimal medium to avoid the influence of dissolved salts on the XPS analysis. Nanoparticles at 1 $mg \cdot mL^{-1}$ concentration were exposed to NADH solutions for 24 h in ~3 mL vials; the samples were then centrifuged (same as above), the supernatant removed, and the remaining nanoparticles particles were rinsed and centrifuged 3× with nanopure water to remove any weakly adsorbed species. The particles were then dried overnight in a vacuum oven. To determine elemental composition on the nanoparticle surfaces, the dried samples were pressed into indium foil and analyzed using a Thermo X-ray photoelectron spectrometer with a monochromatized Al Kα X-ray source and hemispherical analyzer at an angle 45° relative to the surface normal. Survey spectra were obtained summing three scans with a binding energy step size of 1 eV and pass energy of 200 eV, and high-resolution spectra were obtained average 10 (Co(2p)), 20 (O(1s) and C(1s)), or 50 (N(1s) and P(2p)) scans with step size of 0.2 eV and pass energy of 50 eV. Casa XPS software was used for data analysis. For area quantification, peaks were fit to 70:30 Gaussian-Lorentzian functions with Shirley[30] background correction.

## 3. Results and discussion

### 3.1 Nanoparticle characterization

SEM images in Figure 2A-C show relatively monodisperse size and shape within each particle type, with the range in size from $LiCoPO_4$ > $Co(OH)_2$ > $LiCoO_2$. $LiCoO_2$ and $Co(OH)_2$ form hexagonal sheets and $LiCoPO_4$ forms cylindrical rods. Our specific surface area measurements (S) found $S_{LiCoO2}$ = 126.5 ± 0.4 $m^2 \cdot g^{-1}$, $S_{Co(OH)2}$ = 33.29 ± 0.05 $m^2 \cdot g^{-1}$, and $S_{LiCoPO4}$ = 28.1 ± 0.2 $m^2 \cdot g^{-1}$. Differences in these specific surface areas are consistent with sizes observed in SEM. Since most of the experiments reported herein are conducted according to particle mass concentration ($mg \cdot mL^{-1}$), this difference in surface area will be addressed in section 3.3.

Table 1 shows the results of characterizing particles in minimal medium via DLS size and zeta potential. DLS sizes for $LiCoPO_4$ and $Co(OH)_2$ are only slightly larger than compared to what is observed in SEM, indicating minor aggregation. On the other hand, the DLS mean diameter for $LiCoO_2$, is much larger than the primary particles observed in SEM, indicating significant aggregation. All three particle types possess a similarly negative surface charge, which is consistent with all of them being partially deprotonated and/or delithiated in the salt/buffer solution at circumneutral pH.

XRD diffraction patterns of all three particle types are consistent with previously published reference patterns (Figure 2D-F),[31-33] indexed to the $R\bar{3}m$ ($LiCoO_2$), $P\bar{3}m1$ ($Co(OH)_2$) and Cmcm ($LiCoPO_4$) space groups. This agreement indicates that the particles are crystalline and have the correct structure. Slight broadening of XRD peaks is expected given their

nanoscale size.[34] Transmission electron microscopy (TEM) images of $LiCoO_2$ nanosheets before and after exposure to minimal medium reveal a layered structure ~8 nm thick that does not change significantly with solution exposure (Figure S3, ESI†).

**Table 1** Size and surface charge of particles in minimal medium determined from DLS and laser Doppler microelectrophoresis.

| Particle | Mean d (nm) | Zeta potential (mV) |
|---|---|---|
| $LiCoO_2$ | 364 ± 57 | -18.4 ± 0.7 |
| $LiCoPO_4$ | 118 ± 13 | -16.5 ± 3.8 |
| $Co(OH)_2$ | 130 ± 5 | -16.0 ± 2.0 |

### 3.2 Influence of NADH and GSH on Co release

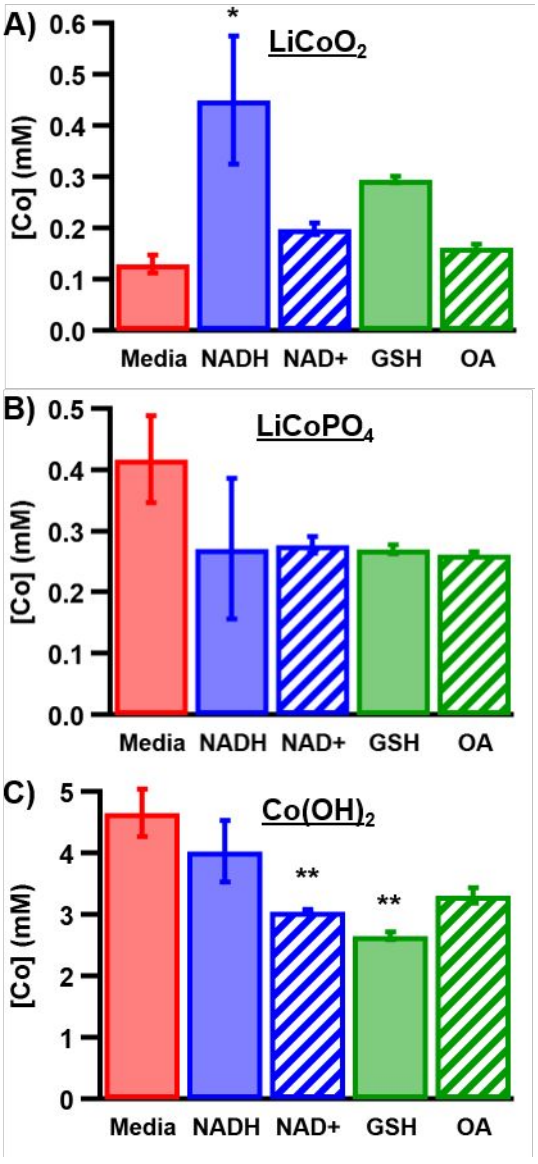


**Figure 3.** Dissolved Co concentrations in minimal medium solutions for A) $LiCoO_2$, B) $LiCoPO_4$, and C) $Co(OH)_2$ after 24-h exposure to each molecule under study. Molecule exposures are compared to media exposure with one-way ANOVA with Dunnett's multiple comparisons test: n = 3 or n = 4, * for $p < 0.05$ and ** for $p < 0.01$.

Figure 3 shows the concentrations of Co measured after $LiCoO_2$, $LiCoPO_4$, and $Co(OH)_2$ nanoparticles were introduced into minimal medium for 24 h. Similar data for Li are included in the ESI† (Figure S4). Figure 3 shows key differences across particles and across solutions tested. Figure 3A shows that exposing $LiCoO_2$ to NADH or GSH increases the release of Co: ~3× increase for NADH and ~2× increase for GSH compared that in minimal medium, with NADH being statistically higher than the media alone at 95% confidence. Since NADH and GSH contain functional groups (carboxylic acid and phosphate groups, respectively) that could complex with Co ions, we conducted further studies using $NAD^+$ and ophthalmic acid (OA). These molecules are nearly identical in structure to NADH and GSA but lack the redox-active functional groups with the ability to reduce Co(III) in $LiCoO_2$. Furthermore, this experiment is necessary because in our experiments (see section 3.5) and in prior studies, phosphate is shown to have affinity for the $LiCoO_2$ surface. Figure 3A shows that $NAD^+$ and OA exposure yields Co concentrations not statistically different from the media alone, and much lower than Co concentrations from NADH or GSH exposure. Based on these results, we conclude that the enhancement produced by NADH and by GSH arises from their oxidation-reduction properties and cannot be attributed to complexation of Co ions with the carboxylate or phosphate groups. Interestingly, NADH shows a greater effect on Co release compared to GSH. By comparing their reduction potentials at pH 7.0 vs. SHE ($E^0_{NADH}$ = -0.320 V[35] and $E^0_{GSH}$ = -0.252 V[36]), NADH is the stronger reducing agent. This is consistent with 1) redox reactivity being the involved in increased Co release and 2) greater enhancement in Co release from NADH exposure compared to GSH exposure.

To further verify that the enhancement in Co release from $LiCoO_2$ induced by NADH and GSH is due to the ability of these molecules to reduce Co(III) (in $LiCoO_2$) to the more highly soluble Co(II), we conducted control experiments using two nanoparticle compositions in which Co exists in a Co(II) state: $LiCoPO_4$ (Figure 3B) and $Co(OH)_2$ (Figure 3C). Figures 3B-C show that for these compositions, the redox-active molecules NADH and GSH as well as the non-redox-active counterparts ($NAD^+$ and OA) do not increase the amount of Co release compared with minimal medium. In the case of $LiCoPO_4$, all molecule exposures lead to slightly lower Co concentrations and none are statistically distinct from Co concentration of media alone at 95% confidence. Exposure to each molecule for $Co(OH)_2$ also shows slight decrease in Co concentration, with $NAD^+$ and GSH statistically different from media alone at 95% confidence. Based on these data, we conclude that the influence of NADH and GSH on $LiCoO_2$ to enhance Co release can be ascribed to their ability to reduce Co(III) to Co(II). The slightly decreased Co release from $Co(OH)_2$ and $LiCoPO_4$ exposed to each molecule compared to with minimal medium alone suggests that these molecules may adsorb to the nanoparticles surfaces and partially restrict ion release (discussed in section 3.5).

Since $LiCoO_2$ and $LiCoPO_4$ are Li intercalation compounds, we also quantified the Li release to examine if it is impacted by the presence of each molecule (ESI†, Figure S4). Dissolved Li concentrations for a given particle in Figure S4 are largely unaffected by changing the composition of the dissolution media. Consistent with prior results, the amount of Li released from these nanoparticles exceed that of Co, due to the fact that $H^+$ ions in solution can exchange with $Li^+$ ions in the solid without involving any redox processes.[37] The $Li^+/H^+$ exchange increases the pH of the solution, as shown by our pH measurements in the ESI†, Table S3. Increase in pH occurs despite the medium being buffered with HEPES due to the high particle concentration (1 mg·mL$^{-1}$) used in our experiments. Notably, the pH values measured after 24-h exposure of $LiCoO_2$ nanoparticles to minimal medium and minimal medium with NADH, $NAD^+$, GSH, and OA are identical within 0.2 pH units. Therefore, we conclude that while $Li^+/H^+$ exchange occurs and increases pH, this process is independent from the mechanism causing enhanced Co release in $LiCoO_2$ in the presence of NADH or GSH and not in the presence of $NAD^+$ or OA.

### 3.3 NADH oxidation during $LiCoO_2$ dissolution

Our results indicate that the enhancement in Co release induced by the presence of NADH or GSH involves reduction of Co(III) to Co(II). In this case, the release of Co should be directly accompanied by an equivalent oxidation of NADH to $NAD^+$ or possibly to other oxidation products. Figure 4 shows the NADH concentration remaining in solution after nanoparticles of the indicated compositions were introduced into the NADH solution for 24 h. These data show that [NADH] greatly decreases with exposure to $LiCoO_2$, slightly decreases with exposure to $Co(OH)_2$, and is statistically unchanged at 95% confidence when exposed to $LiCoPO_4$. Also shown in Figure 4 are results from control samples prepared in an identical manner except lacking NADH; these samples show no significant fluorescence. We attribute the large decrease in [NADH] with $LiCoO_2$ to the oxidation of NADH coupled with Co release from LiCoO2. The slight decrease in observed [NADH] with $Co(OH)_2$ exposure is consistent with our results in Figure 7B showing NADH adsorbing onto the surface of $Co(OH)_2$, as any adsorbed molecules would be removed from the solution with the particles before fluorescence analysis (see section 3.5).

Considering that the specific surface area of $LiCoO_2$ particles (126.5 ± 0.4 $m^2 \cdot g^{-1}$) is approximately 4 - 4.5 times the specific surface areas of $Co(OH)_2$ (33.29 ± 0.05 $m^2 \cdot g^{-1}$) and $LiCoPO_4$ (28.1 ± 0.2 $m^2 \cdot g^{-1}$), we performed $LiCoPO_4$ dissolution experiments normalized by surface area instead of mass (i.e. 4.5× $LiCoPO_4$ particle concentration) to ensure that selective loss of NADH is not simply a surface area effect. The resulting [NADH] measured by fluorescence is shown in Figure 4 as "*$LiCoPO_4$". The [NADH] for surface area normalized *$LiCoPO_4$ samples is nearly identical to the [NADH] for mass-normalized $LiCoPO_4$ and $Co(OH)_2$ samples and much higher than that for $LiCoO_2$ samples. This shows that the differences in dissolution behavior and

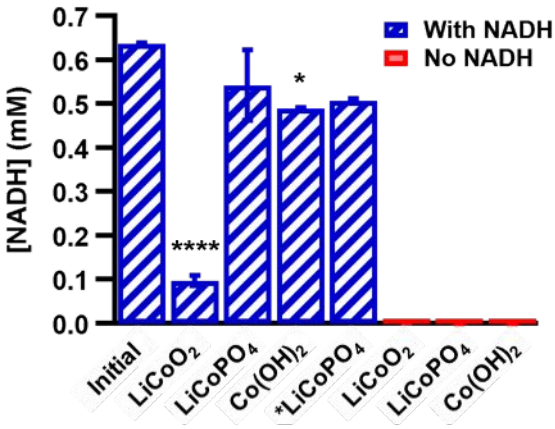


**Figure 4.** Concentration of NADH before ("initial") and after exposure to the indicated nanoparticles for 24 h. "*$LiCoPO_4$" refers to NADH solutions after 24-h exposure to 4.5 × [LiCoPO4], a matching specific surface area exposure to $LiCoO_2$ samples. Particle solutions are compared to initial with one-way ANOVA with Dunnett's multiple comparisons test: n = 2 or n = 3, * for $p < 0.05$ and *** for $p < 0.0001$. Also shown are fluorescence intensities of control samples prepared in an identical manner but without NADH ("No NADH").

biomolecule interactions between $LiCoO_2$ and $LiCoPO_4/Co(OH)_2$ are due to differences in their chemical properties, not differences in surface areas.

While we anticipate that loss of NADH fluorescence is caused by oxidation to $NAD^+$, we also considered whether loss of NADH might be cause by several other phenomena, including 1) a reaction of NADH with dissolved $Co^{2+}$ or $Li^+$ ions, 2) adsorption of NADH onto the filter used to remove particles, and 3) interference in fluorescence spectra from residual particles scattering light. Details of these control experiments are presented in the ESI† (Figure S5). Notably, exposing NADH solution to dissolved $Co^{2+}/Li^+$ ions similar in concentration to experimental solutions or passing NADH solution through the syringe filter show no appreciable decrease in their fluorescence intensities. These control experiments uniformly confirm that NADH is oxidized to $NAD^+$ by the nanoparticles.

As a complement to measuring the loss of NADH by fluorescence, we also used UV-visible absorption spectra of NADH solutions with/without exposure to $LiCoO_2$, $LiCoPO_4$ and $Co(OH)_2$ to assess the concentrations of NADH and $NAD^+$ before/after nanoparticle exposure. NADH and $NAD^+$ both exhibit peaks around 203 nm and 259 nm with similar molar absorptivities, whereas NADH alone exhibits a peak at 339 nm.[38] The ESI† contains a detailed analysis of NADH and $NAD^+$ UV-visible absorbance spectra (Figure S6). Interestingly, we found concentration-dependent peak shifts at higher concentrations, perhaps due to molecule aggregation/stacking. Based on their spectral properties, we can identify the redox state of a NADH/$NAD^+$ solution using absorbances at 259 nm and 339 nm. For a NADH solution exposed to particles, the three possible cases are: 1) to retain absorbance at 339 nm, NADH has not been transformed to $NAD^+$, removed, or degraded, 2) to lose absorbance at 339 nm but retain absorbance at 259 nm, NADH

 

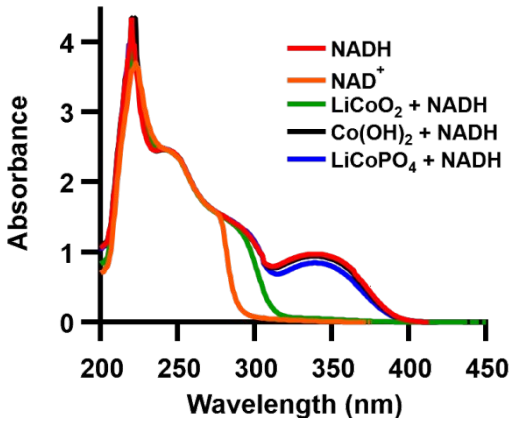


**Figure 5.** UV-visible absorption spectra of 0.5 mM solutions of NADH and $NAD^+$, and 0.5 mM NADH solutions after 24-h exposure to $LiCoO_2$, $LiCoPO_4$, and $Co(OH)_2$. All solutions were prepared in minimal medium, which also served as the background. All 0.5 mM $NAD^+$ samples exposed to nanoparticles yielded spectra nearly identical to the orange "$NAD^+$" trace without nanoparticle exposure and are omitted for clarity.

has been oxidized to $NAD^+$, or 3) to lose absorbance at both 339 nm and 259 nm, NADH has been removed from the system or severely degraded. Figure 5 shows a clear difference in which case is followed between solutions exposed to $LiCoO_2$ compared to solutions exposed to $LiCoPO_4$ or $Co(OH)_2$. With exposure to $LiCoPO_4$ or $Co(OH)_2$, NADH solutions maintain absorbance at 339 nm and 259 nm, indicating that NADH is unchanged (case #1). With exposure to $LiCoO_2$, absorbance at 339 nm is almost entirely lost, while absorbance at 259 nm is constant (case #2). Therefore, our UV-visible absorption results support the conclusion that NADH is oxidized to $NAD^+$ with $LiCoO_2$ exposure, but not with $LiCoPO_4$ or $Co(OH)_2$ exposure. Since these data suggest $NAD^+$ was present in our prior fluorescence studies, we confirmed that solutions of $NAD^+$ with/without nanoparticle exposure yield negligible fluorescence compared to NADH solutions (Figure S7, ESI†).

Since NADH/$NAD^+$ absorbance properties change with concentration, particularly at the 500 µM used for most dissolution experiments, additional dissolution experiments identical to those described in the experimental were performed exposing $LiCoO_2$ to 100 µM NADH in minimal medium. The results combining $LiCoO_2$ and 100 µM NADH show a decrease in [NADH] measured by fluorescence from 91.6 ± 6.6 µM to 2.21 ± 0.19 µM, and an increase in released Co measured by ICP-MS from 0.120 ± 0.002 mM to 0.139 ± 0.006 mM. These changes reaffirm that NADH enhances Co release and $LiCoO_2$ oxidizes NADH. Since results are consistent across the NADH concentrations tested, we conclude that the increase in released Co and oxidation of NADH at higher concentrations is not due to some specific spectral or aggregation effect of NADH, but through interaction with $LiCoO_2$.

The relative magnitudes of changes in NADH removal and Co release for 100 µM NADH are different compared to those of the 500 µM NADH experiments (i.e. Figures 3 and 4) because

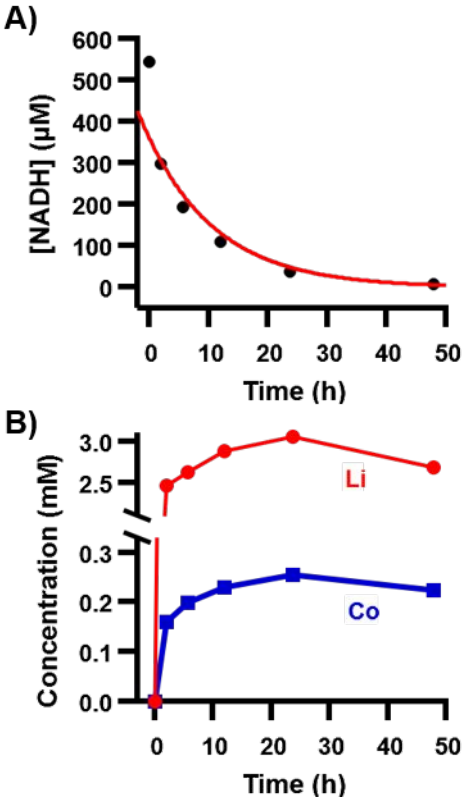


**Figure 6.** Concentrations measured over time for species in dissolution of 1 mg·mL$^{-1}$ $LiCoO_2$ with 0.5 mM NADH A) NADH measured by fluorescence with exponential decay fit of $Y = 350 \cdot e^{-0.084 \cdot X}$, and B) concentrations of Li (red circles) and Co (blue squares) measured by ICP-MS.

in the case of 100 µM, [$LiCoO_2$] ≈ 100×[NADH], whereas in the case of 500 µM, [$LiCoO_2$] ≈ 20×[NADH] (1 mg·mL$^{-1}$ $LiCoO_2$ for both). That is, in the extreme where [$LiCoO_2$] >> [NADH], a given amount of reaction yields a relatively large change in [NADH] and a relatively small change in released Co concentration.

### 3.4 Reaction kinetics of NADH and $LiCoO_2$

To characterize the kinetics of the interaction between NADH and $LiCoO_2$, we measured the concentrations of NADH (reactant) and released Co (product) over time for a single reaction solution. Time-points were taken from 2-hr to 48-hr, spanning across the 24-hr time point used in other experiments. The data in Figure 6A reveal an exponential decrease in [NADH] over the course of reaction. The general rate equation for this reaction is described by Eq. 1:

$$\frac{d[NADH]}{dt} = k[NADH]^n[LiCoO_2]^m \quad (1)$$

where $k$ is the rate constant and $n$ and $m$ are reaction orders for NADH and $LiCoO_2$, respectively. As noted above, under the conditions of our experiments we assume [$LiCoO_2$] >> [NADH] and Δ[$LiCoO_2$] ≈ 0. Because of this, even if $m \neq 0$ the rate expression in Eq. 1 can be simplified by combining [$LiCoO_2$]$^m$ within the rate constant, $k$:

$$\frac{d[NADH]}{dt} \approx k'[NADH]^n \quad (2)$$

From curve fitting graphs of [NADH], ln[NADH], and $[NADH]^{-1}$ vs. time, it is clear that the reaction is first order with respect to NADH (i.e. $n = 1$). For example, in the case of ln[NADH] vs. time a linear regression yields $R^2 = 0.972$, whereas for [NADH] vs. time linear $R^2 = 0.581$. We determined the pseudo-first-order rate constant of $k' = 0.084 \pm 0.007$ $hr^{-1}$. Interestingly, the t = 0 point in Figure 6A deviates more significantly from the fit than most points. This suggests that a separate process, possibly adsorption of NADH onto the particles (see section 3.5) occurs in the initial stages of dissolution to remove more NADH than expected over the longer-term reaction.

Concentrations of dissolved Co and Li for the same dissolution experiment are shown in Figure 6B. As with single time point experiments, [Li] >> [Co] due to $Li^+$-proton exchange. Both species are released at a greater rate in the initial stages of reaction, and plateau in concentration over time. The plot of Co concentration with time mirrors that of NADH with time, which we ascribe to solubilized Co being a product of the reaction of NADH with $LiCoO_2$. The decrease in the rate of Co-production with time is consistent with our conclusion that the NADH-$LiCoO_2$ reaction depends directly on [NADH].

### 3.5 Binding of NADH to nanoparticles

The data in Figures 3 and 4 suggest that some of the apparent loss of NADH is due to adsorption onto the nanoparticle surfaces. Additionally, the sharp decrease in [NADH] at the first time point of our kinetics study suggests NADH adsorbs relatively quickly compared to the longer-term redox reaction. To determine the extent of NADH interaction with nanoparticle surfaces, we obtained XPS spectra of nanoparticles before and after exposure to NADH, using N(1s) emission to quantify the presence of NADH and using Co(2p) as an internal standard. Figure 7A shows representative N(1s) spectra from $LiCoO_2$ before and after exposure to NADH (0.5 mM, 24 h). Additional spectra are shown in the ESI†. Figure 7A clearly shows a pronounced increase in N(1s) emission intensity for the NADH-exposed sample compared to the unexposed sample. Figure 7B summarizes similar data for $LiCoO_2$, $LiCoPO_4$, and $Co(OH)_2$. We note that while NADH is the species introduced to the nanoparticles, the XPS spectra cannot distinguish between adsorbed NADH or $NAD^+$. We determined the surface coverage of N atoms bound to each surface ($LiCoO_2$, $LiCoPO_4$, and $Co(OH)_2$) from the N(1s) and Co(2p) photoelectron emission (Figure 7B), as described in the ESI†. Figure 7B shows the resulting surface coverages. The data show a statistically significant increase in N surface coverage with NADH exposure for $Co(OH)_2$ at 95% confidence, a moderate increase for $LiCoO_2$, and no change for $LiCoPO_4$. Using the known stoichiometry of 7 N atom per NADH/$NAD^+$ molecule, the N coverages correspond to $0.37 \pm 0.07$ NADH/$NAD^+$ molecule·$nm^{-2}$ for $LiCoO_2$, $0.036 \pm 0.007$ molecule·$nm^{-2}$ for $LiCoPO_4$, and $0.62 \pm 0.05$ molecule·$nm^{-2}$ for $Co(OH)_2$. For comparison, assuming a density of closely packed NADH of ~1.7 g·$cm^{-3}$ (from solid NADH) and monolayer thickness of ~0.5 nm yields a maximum coverage of ~0.8 molecule·$nm^{-2}$. A 0.5 nm monolayer thickness is estimated using literature[39] bond lengths and assuming a monolayer of NADH/$NAD^+$ molecules bind via a phosphate moiety (see below) in a planar conformation roughly perpendicular to the surface. Thus, on $LiCoO_2$ and $Co(OH)_2$ the molecular coverages estimated from XPS are comparable to that expected from a monolayer of NADH/$NAD^+$.

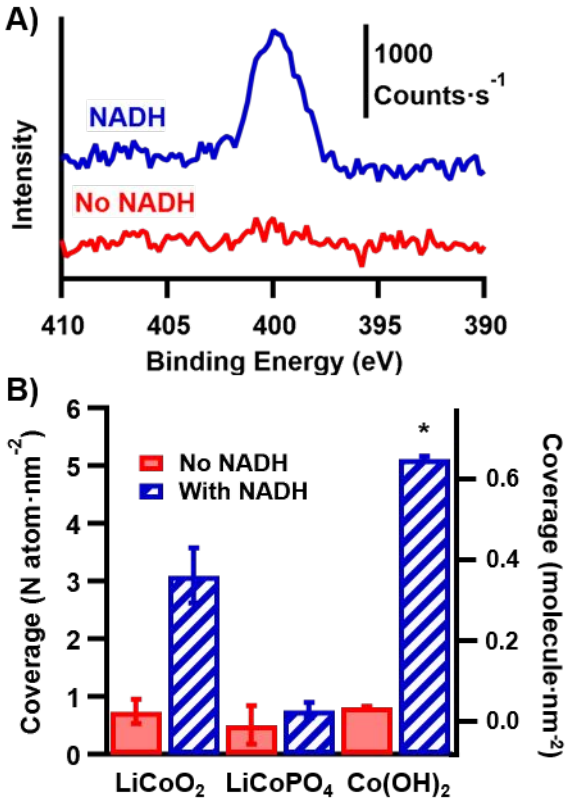


**Figure 7.** A) N(1s) XPS spectra of $LiCoO_2$ particles after 24-h soak in solutions with or without 0.5 mM NADH, and B) N atom surface coverages on nanoparticles after 24-h soak with or without 0.5 mM NADH, determined from N(1s) and Co(2p) peak areas. With/without NADH samples are compared for a given particle type with unpaired t-test with Welch's correction: n = 2 or n = 3, * for $p < 0.05$.

The presence of significant N coverage after three cycles of rinsing, mixing, and centrifuging indicates that NADH/$NAD^+$ has a high affinity with $LiCoO_2$ and $Co(OH)_2$ surfaces. The strong binding we observe for NADH/$NAD^+$ with $LiCoO_2$ and $Co(OH)_2$ suggests that the phosphate moieties in NADH/$NAD^+$ bind to surface oxygen atoms on each particle surface, and that the phosphate-containing molecules do not bind to phosphate terminated particles (i.e. $LiCoPO_4$). This result is an agreement with prior work showing that phosphate binds strongly to $LiCoO_2$[21] and to Fe(III) oxides[40] via an inner-sphere configuration on an oxygen-terminated surface. Notably, prior work reported that despite its attachment to the $LiCoO_2$ surface, phosphate does not increase $LiCoO_2$ dissolution.[21] In contrast, we find that NADH significantly increases $LiCoO_2$ dissolution. Using our measured $LiCoO_2$ specific surface area, XPS surface density, and known solution volumes, we determined that adsorption onto

the $LiCoO_2$ nanoparticle surfaces accounts for decrease in total NADH concentration of (0.077 ± 0.014 mM). This value is much smaller than the actual decrease in [NADH] after 24-h $LiCoO_2$ exposure (0.539 ± 0.012 mM) that we observed and allows us to conclude that while NADH binds to $LiCoO_2$ nanoparticle surfaces, surface adsorption is not the primary origin of the decrease in [NADH] observed in Figures 4 and 5. On the other hand, the fact that NADH binds even more strongly with $Co(OH)_2$ can explain the much smaller decrease in [NADH] seen in Figure 4. Any NADH molecules adhering to the $Co(OH)_2$ particles are removed from the solution and would not contribute to the measured fluorescence.

### 3.6 Coupled transformation of NADH and $LiCoO_2$

The data in Figure 3 show that in minimal medium alone (i.e., in the absence of NADH or other intentionally added reducing agents), the amount of Co released from $LiCoO_2$ is much less than the amount released from $LiCoPO_4$. This observation is consistent with the hypothesis that while $LiCoPO_4$ can directly release cobalt in the highly soluble Co(II) form, release of cobalt from $LiCoO_2$ is less favorable due to the highly insoluble nature of Co(III). The lower rate of release from $LiCoO_2$ in the absence of added reducing agents is further supported by density functional theory (DFT) and thermodynamics calculations of the initial steps (loss of first partial-monolayer) in release of Co from the lowest-energy surface faces of $LiCoO_2$ and $LiCoPO_4$ in water. These calculations (see ESI†) indicate that the initial release of Co from the $LiCoO_2$(001) surfaces in pure water at pH = 7 (with other water-soluble species set at $10^{-6}$ M) is endergonic with an energy change of ΔG = +1.15 eV/Co while initial release from the $LiCoPO_4$(010) surface is exergonic, ΔG = -0.87 eV/Co, in qualitative agreement the experimental results.

Our experiments demonstrate that NADH greatly increased the rate of Co release from $LiCoO_2$, while no corresponding increase release from $LiCoPO_4$. This observation strongly points to an electrochemically driven interaction between NADH and $LiCoO_2$. The electrochemical reduction of $LiCoO_2$ with release of $Co^{2+}$ can be described via the half-cell reaction:

$$LiCoO_{2(s)} + 4H^+_{(aq)} + e^- \rightleftharpoons Li^+_{(aq)} + Co^{2+}_{(aq)} + 2H_2O_{(l)} \quad (3)$$

$$E^0_{(SHE)} = 2.14\ V$$

Here, the standard electrochemical reduction potential of $E^0$ = +2.14 V at 25°C can be readily determined using the Gibbs free energy of formation of $LiCoO_2$ from the pure elements at standard state (-615 kJ·mol$^{-1}$)[41, 42] and standard electrochemical potentials. The $NADH/NAD^+$ couple is described by the electrochemical reduction:[35]

$$NAD^+_{(aq)} + H^+_{(aq)} + 2e^- \rightleftharpoons NADH_{(aq)} \quad (4)$$

$$E^0_{(SHE)} = -0.315\ V$$

Coupling these two together to form the electrochemically mediated reaction (Eq. 5) yields a net ΔG = -4.9 eV (-474 kJ·mol$^{-1}$) as written, or -2.45 eV per $Co^{2+}$ ion released.

$$2LiCoO_{2(s)} + 7H^+_{(aq)} + NADH_{(aq)} \rightleftharpoons 2Li^+_{(aq)} + 2Co^{2+}_{(aq)} + 4H_2O_{(l)} + NAD^+_{(aq)} \quad (5)$$

Additionally, our measurements of [NADH] vs. time and [Co] vs. time demonstrate the reaction is first order with respect to NADH and that the reaction rate is greatest when nanoparticles and NADH solution are first exposed to one another. While the stoichiometry of Eq. 5 suggests there should be two Co ions released for each molecule of NADH that is reduced, experimentally we observe that the Co release (0.32 ± 0.13 mM) is smaller than the loss of NADH (loss of 0.539 ± 0.012 mM). This greater than anticipated loss of NADH suggests that NADH may be simultaneously involved in other reduction reactions, such as:

$$NADH + H^+ \rightleftharpoons NAD^+ + H_{2(g)} \quad (6)$$

with $\Delta G^0$ = +0.037 eV. A prior study reported evidence for direct surface oxidation of NADH at $Co_3O_4$ surfaces,[43] while other studies have shown that oxides made from metal oxides exhibit enhanced electrochemical reduction of NADH and have attributed this enhancement to the ability of metal oxide surfaces to adsorb protons.[43] As a result, we conclude that while release of Co(II) is directly attributed to NADH, the transformation of NADH and $NAD^+$ may be further increased by additional surface-catalyzed reactions.

## 4. Conclusions

Our results show that biological molecules that are important in cellular respiration and electron transport can play an active role in the transformation of high-valence transition metal oxides through redox chemistry at nanoparticle surfaces. NADH and GSH interact with $LiCoO_2$ nanoparticles by redox chemistry at the solid-liquid interface: electrochemical reduction of Co(III) to Co(II) allows Co to be easily solubilized and released into solution while also oxidizing NADH to $NAD^+$. We attribute this coupled redox transformation to redox reaction between Co(III) within $LiCoO_2$ and NADH/GSH reducing agents, and not a complexation/chelation/pH effect, based on five pieces of evidence. First, NADH and GSH produce similar effects when exposed to $LiCoO_2$ despite differences in their structures. Second, non-reducing analogues of NADH and GSH do not reproduce the same effects. Third, NADH is oxidized when exposed to $LiCoO_2$ but not when exposed to $LiCoPO_4$ or $Co(OH)_2$ (whether samples are normalized by mass or surface area) and is not oxidized when exposed to $Co^{2+}/Li^+$ ions. Fourth, Li release is relatively unaffected by the presence of the molecules, as this occurs primarily by $H^+$ exchange, and pH change is found to not be the driver of changes in dissolution in our experiments. Lastly, measuring concentrations of NADH (reactant) and released Co (product) over time reveal a direct relationship between reaction rate and [NADH].

Transformations of nanoparticles driven by redox chemistry of molecules involved in biological electron transport pose two important mechanisms for toxicity in the environment. First, the reduction of Co(III) and other high valence metals to lower-valence states increases their solubility and leads to faster release into the aqueous phase. High concentrations of metals such as Co and Ni released from metal oxides have been shown

to induce toxicity towards various aquatic organisms.[44, 45] Select microorganisms (e.g. *S. oneidensis* MR-1) are known to reduce high valent metals (Fe, Co, Mn) in minerals extracellularly,[46] increasing metal ion release.[47-49] We find similar behavior from introduction of reducing biomolecules, suggesting that this metal-reduction phenomenon could occur to a lesser extent from non-metal-reducing organisms interacting with high surface area nano-scale metal oxides. Secondly, the corresponding oxidation of NADH, GSH, and other molecules relevant to electron transport and cellular homeostasis can serve as an additional pathway to biological impact. When redox-active molecules facilitate metal oxide nanoparticle dissolution, they can be transformed or degraded. In the case of NADH and GSH, severe unnatural oxidation surrounding a non-metal-reducing organism from interaction with a nanoparticle will alter the NADH:$NAD^+$ and GSH:GSSG ratios in/around cells, entirely disrupting cellular redox homeostasis. Imbalances in GSH or NADH concentrations can have many toxic effects,[50] but in particular, removal of the reduced forms of these well-known antioxidants may lower cellular defenses against ROS. Several studies have observed ROS in the presence of nanomaterials,[51, 52] including $LiCoO_2$.[53] In such cases, whether nanoparticle transformation or cellular machinery generates ROS, the ROS will more negatively impact cells with reduced anti-oxidant capability.

## Conflicts of interest

There are no conflicts to declare.

## Acknowledgements

This material is based upon work supported by the National Science Foundation under Grant No. CHE-2001611, the NSF Center for Sustainable Nanotechnology. The CSN is part of the Centers for Chemical Innovation Program.

The authors gratefully acknowledge use of University of Wisconsin facilities and instrumentation through the Research Science and Engineering Center (partially supported through NSF DMR-1720415) and Water Science and Engineering Laboratory. The authors also acknowledge Dr. Pamela Doolittle for assistance with ICP-MS measurements.

## References

1 M. N. Hang, I. L. Gunsolus, H. Wayland, E. S. Melby, A. C. Mensch, K. R. Hurley, J. A. Pedersen, C. L. Haynes and R. J. Hamers, Impact of nanoscale lithium nickel manganese cobalt oxide (NMC) on the bacterium *Shewanella oneidensis* MR‐1, *Chem. Mater.,* 2016, **28**, 1092-1100.

2 M. N. Hang, N. V. Hudson-Smith, P. L. Clement, Y. Zhang, C. Wang, C. L. Haynes and R. J. Hamers, Influence of nanoparticle morphology on ion release and biological impact of nickel manganese cobalt oxide (NMC) complex oxide nanomaterials, *ACS App.. Nano Mater.*, 2018, **1**, 1721-1730.

3 J. I. Drever and L. L. Stillings, The role of organic acids in mineral weathering, *Coll. Surf. A: Phys. Eng. Aspects*, 1997, **120**, 167-181.

4 W. H. Huang and W. D. Keller, Dissolution of rock-forming silicate minerals in organic acids: simulated first-stage weathering of fresh mineral surfaces, Am. Mineral., 1970, **55**, 2076-2094.

5 G. J. Houben, Iron oxide incrustations in wells. Part 2: chemical dissolution and modeling, *Appl. Geochem.*, 2003, **18**, 941-954.

6 E. D. Flynn and J. G. Catalano, Reductive transformations of layered manganese oxides by small organic acids and the fate of trace metals, *Geochim. Cosmochim. Acta*, 2019, **250**, 149-172.

7 B. Gu, W. Dong, L. Liang and N. A. Wall, Dissolution of technetium(iv) oxide by natural and synthetic organic ligands under both reducing and oxidizing conditions, *Environ. Sci. Technol.* , 2011, **45**, 4771-4777.

8 G. E. Brown, V. E. Henrich, W. H. Casey, D. L. Clark, C. Eggleston, A. Felmy, D. W. Goodman, M. Gratzel, G. Maciel, M. I. McCarthy, K. H. Nealson, D. A. Sverjensky, M. F. Toney and J. M. Zachara, Metal oxide surfaces and their interactions with aqueous solutions and microbial organisms, *Chem. Rev.*, 1999, **99**, 77-174.

9 K. H. Nealson and D. Saffarini, Iron and manganese in anaerobic respiration - environmental significance, physiology, and regulation, *Ann. Rev. Microbiol.*, 1994, **48**, 311-343.

10 S. K. Lower, M. F. Hochella and T. J. Beveridge, Bacterial recognition of mineral surfaces: Nanoscale interactions between *Shewanella* and alpha-FeOOH, *Science*, 2001, **292**, 1360-1363.

11 X. Zeng, J. Li and L. Liu, Solving spent lithium-ion battery problems in China: Opportunities and challenges, *Renewable and Sustainable Energy Reviews*, 2015, **52**, 1759-1767.

12 D. Beyersmann and A. Hartwig, Carcinogenic metal compounds: Recent insight into molecular and cellular mechanisms, *Arch. Toxicol.*, 2008, **82**, 493-512.

13 D. J. Paustenbach, B. E. Tvermoes, K. M. Unice, B. L. Finley and B. D. Kerger, A review of the health hazards posed by cobalt, *Crit. Rev. Toxicol.*, 2013, **43**, 316-362.

14 K. H. Gayer and A. B. Garrett, The solubility of cobalt hydroxide, $Co(OH)_2$, in solutions of hydrochloric acid and sodium hydroxide at 25 Degrees, *J. Am. Chem. Soc.*, 1950, **72**, 3921-3923.

15 J. Chivot, L. Mendoza, C. Mansour, T. Pauporte and M. Cassir, New insight in the behaviour of Co-$H_2O$ system at 25-150 degrees C, based on revised Pourbaix diagrams, *Corrosion Sci.*, 2008, **50**, 62-69.

16 S.-J. Lin and L. Guarente, Nicotinamide adenine dinucleotide, a metabolic regulator of transcription, longevity and disease, *Curr. Opin. Cell Biol.*, 2003, **15**, 241-246.

17 H. Sies, Glutathione and its Role in Cellular Functions, *Free Radical Biology & Medicine*, 1999, **27**, 916-921.

18 X. Liu, S. Sen, J. Liu, I. Kulaots, D. Geohegan, A. Kane, A. A. Puretzky, C. M. Rouleau, K. L. More, G. T. R. Palmore and R. H. Hurt, Antioxidant deactivation on graphenic nanocarbon surfaces, *Small*, 2011, **7**, 2775-2785.

19 Y. Wang, Y. Basdogan, T. Zhang, R. S. Lankone, A. N. Wallace, D. H. Fairbrother, J. A. Keith and L. M. Gilbertson,

Unveiling the synergistic role of oxygen functional groups in the graphene-mediated oxidation of glutathione, ACS *Appl. Mater. Interface.*, 2020, **12**, 45753-45762.

20 E. D. Laudadio, P. Ilani-kashkouli, C. M. Green, N. J. Kabengi and R. J. Hamers, Interaction of phosphate with lithium cobalt oxide nanoparticles: A combined spectroscopic and calorimetric study, *Langmuir*, 2019, **35**, 16640-16649.

21 E. D. Laudadio, J. W. Bennett, C. M. Green, S. E. Mason and R. J. Hamers, Impact of Phosphate Adsorption on Complex Cobalt Oxide Nanoparticle Dispersibility in Aqueous Media, *Environ. Sci. Technol.*, 2018, **52**, 10186-10195.

22 K. J. Kreder III, G. Assat and A. Manthiram, Microwave-Assisted Solvothermal Synthesis of Three Polymorphs of $LiCoPO_4$ and Their Electrochemical Properties, *Chem. Mater.*, 2015, **27**, 5543-5549.

23 S. Brunauer, P. H. Emmett and E. Teller, Adsorption of Gases in Multimolecular Layers, *J. Am. Chem. Soc.*, 1938, **60**, 309-319.

24 W. Xiao, R. S. Wang, D. E. Handy and J. Loscalzo, NAD(H) and NADP(H) Redox Couples and Cellular Energy Metabolism, *Antioxidants and Redox Signaling*, 2018, **28**, 251-272.

25 P. D. Reiss, P. F. Zuurendonk and R. L. Veech, Measurement of tissue purine, pyrimidine, and other nucleotides by radial compression high-performance liquid chromatography, *Anal. Biochem.*, 1984, **140**, 162-171.

26 K. Yamada, N. Hara, T. Shibata, H. Osago and M. Tsuchiya, The simultaneous measurement of nicotinamide adenine dinucleotide and related compounds by liquid chromatography / electrospray ionization tandem mass spectrometry, *Analy. Biochem.*, 2006, **352**, 282-285.

27 G. Wu, Y.-z. Fang, S. Yang, J. R. Lupton and N. D. Turner, Glutathione metabolism and its implications for health, *J. Nutrition*, 2004, **134**, 489-492.

28 B. Chance, B. Schoener, R. Oshino, F. Itshak and Y. Nakase, Oxidation-reduction ratio studies of mitochondria in freeze-trapped samples, *J. Biological Chem.*, 1979, **254**, 4764-4771.

29 A. U. Rehman, A. G. Anwer, M. E. Gosnell, S. B. Mahbub, G. Liu and E. M. Goldys, Fluorescence quenching of free and bound NADH in HeLa cells determined by hyperspectral imaging and unmixing of cell autofluorescence, *Biomed. Opt. Express*, 2017, **8**, 1488-1498.

30 D. A. Shirley, High-resolution X-ray Photoemission spectrum of the valence bands of gold, *Phy. Rev. B*, 1972, **5**, 4709-4714.

31 Y. Takahashi, N. Kijima, K. Dokko, M. Nishizawa, I. Uchida and J. Akimoto, Structure and electron density analysis of electrochemically and chemically delithiated $LiCoO_2$ single crystals, *J. Solid State Chem.*, 2007, **180**, 313-321.

32 W. Lotmar and W. Feitknecht, Uber Anderungen derlonenabstande in hydroxd-schichtengittern, *Zeitschrift fur Kristallographie*, 1936, **93,** 368-378

33 G. Bergerhoff and I. D. Brown, Crystallographic Databases, F. H. Allen, ed., Int. Union of Crystallography, Chester, 1987.

34 D. G. Lamas, M. D. O. Neto, G. Kellermann and A. F. Craievich, X-ray Diffraction and Scattering by Nanomaterials, in Nanocharacterization Techniques, Elsevier Inc., 2017, pp. 111-182.

35 D. F. Wilson, M. Erecinska and P. L. Dutton, Thermodynamic relationships in mitochondrial oxidative phosphorylation, *Ann. Rev. Biophys. Bioeng.*, 1974, **3**, 203-230.

36 K. K. Millis, K. H. Weaver and D. L. Rabenstein, Oxidation / reduction potential of glutathione, *J. Org. Chem.* 1993, **58**, 4144-4146.

37 I. A. Shkrob, J. A. Gilbert, P. J. Phillips, R. Klie, R. T. Haasch, J. Bareño and D. P. Abraham, Chemical weathering of layered Ni-rich oxide electrode materials: evidence for cation exchange, *J. Electrochem. Soc.,* 2017, **164**, A1489-A1498.

38 L. M. Blank, B. E. Ebert, K. Buehler and B. Bühler, Redox biocatalysis and metabolism: Molecular mechanisms and metabolic network analysis, *Antioxidants and Redox Signaling*, 2010, **13**, 349-394.

39 R. D. Johnson III, Computational Chemistry Comparison and Benchmark Database, National Institute of Standards and Technology, 2019.

40 R. A. Berner, Phosphate Removal from Sea Water by Adsorption on Volcanogenic Ferric Oxides, *Earth and Planetary Science Letters*, 1973, **18**, 77-86.

41 M. Wang and A. Navrotsky, Enthalpy of formation of $LiNiO_2$, $LiCoO_2$ and their solid solution, $LiNi_{1-x}Co_xO_2$, *Solid State Ionics*, 2004, **166**, 167-173.

42 H. Yokokawa, N. Sakai, K. Yamaji, T. Horita and M. Ishikawa, Thermodynamic determining factors of the positive electrode potential of lithium batteries, *Solid State Ionics*, 1998, **113**, 1-9.

43 C. H. Chen, Y. C. Chen and M. S. Lin, Amperometric determination of NADH with $Co_3O_4$ nanosheet modified electrode, *Biosens. Bioelectron.*, 2013, **42**, 379-384.

44 G. E. Batley, J. K. Kirby and M. J. McLaughlin, Fate and risks of nanomaterials in aquatic and terrestrial environments, *Acc. Chem. Res.*, 2013, **46**, 854-862.

45 W. H. R. Shaw, Cation Toxicity and the Stability of Transition-Metal Complexes, *Nature*, 1961, **192**, 754-755.

46 L. Shi, H. Dong, G. Reguera, H. Beyenal, A. Lu, J. Liu, H. Q. Yu and J. K. Fredrickson, Extracellular electron transfer mechanisms between microorganisms and minerals, *Nature. Rev. Microbiol.*, 2016, **14**, 651-662.

47 J. R. Lloyd, Microbial reduction of metals and radionuclides, *FEMS Microbiol. Rev.* , 2003, **27**, 411-425.

48 Y. A. Gorby, F. Caccavo and H. Bolton, Microbial reduction of Cobalt(III) $EDTA^-$ in the presence and absence of manganese(IV) oxide, *Environ. Sci. Technol.* , 1998, **32**, 244-250.

49 F. Caccavo, D. J. Lonergan, D. R. Lovley, M. Davis, J. F. Stolz and M. J. McInerney, *Geobacter sulfurreducens sp. nov.*, a hydrogen- and acetate-oxidizing dissimilatory metal-reducing microorganism, *Appl. Env. Microbiol.*, 1994, **60**, 3752-3759.

50 W. Ying, $NADH^+$ and NADH in Cellular Functions and Cell Death, *Frontiers in Bioscience*, 2006, **11**, 3129-3148.

51 E. Papis, F. Rossi, M. Raspanti, I. Dalle-Donne, G. Colombo, A. Milzani, G. Bernardini and R. Gornati, Engineered cobalt oxide nanoparticles readily enter cells, *Toxicol. Lett.*, 2009, **189**, 253-259.

52 B. Behl, I. Papageorgiou, C. Brown, R. Hall, J. L. Tipper, J. Fisher and E. Ingham, Biological effects of cobalt-chromium

nanoparticles and ions on dural fibroblasts and dural epithelial cells, *Biomater.*, 2013, **34**, 3547-3558.

53 E. S. Melby, Y. Cui, J. Borgatta, A. C. Mensch, M. N. Hang, B. Chrisler, A. Dohnalkova, J. M. V. Gilder, C. M. Alvarez, J. N. Smith, R. J. Hamers and G. Orr, Impact of lithiated cobalt oxide and phosphate nanoparticles on rainbow trout gill epithelial cells, *Nanotoxicol.*, 2018, **12**, 1166-1181.